Use of a Liquid-Crystal, Heater-Element Composite for Quantitative, High-Resolution Heat Transfer Coefficients on a Turbine Airfoil, Including Turbulence and Surface Roughness Effects

Steven A. Hippensteele, Louis M. Russell,
and Felix J. Torres

May 1987

NASA

Use of a Liquid-Crystal, Heater-Element Composite for Quantitative, High-Resolution Heat Transfer Coefficients on a Turbine Airfoil, Including Turbulence and Surface Roughness Effects

Steven A. Hippensteele, Louis M. Russell,
and Felix J. Torres
Lewis Research Center
Cleveland, Ohio

NASA

National Aeronautics and
Space Administration

Lewis Research Center
Cleveland, Ohio 44135

Summary

Local heat transfer coefficients were measured along the midchord of a three-times-size turbine vane airfoil in a static cascade operated at room temperature over a range of Reynolds numbers. The test surface consisted of a composite of commercially available materials: a Mylar sheet with a layer of cholesteric liquid crystals, which change color with temperature, and a heater made of a polyester sheet coated with vapor-deposited gold, which produces uniform heat flux. After the initial selection and calibration of the composite sheet accurate, quantitative, and continuous heat transfer coefficients were mapped over the airfoil surface. Tests were conducted at two free-stream turbulence intensities: 0.6 percent, which is typical of wind tunnels; and 10 percent, which is typical of real engine conditions. In addition to a smooth airfoil the effects of local leading-edge sand roughness were also examined for a value greater than the critical roughness (the minimum roughness that causes transition in a laminar boundary layer). The local heat transfer coefficients are presented for both free-stream turbulence intensities for inlet Reynolds numbers from 1.20×10^5 to 5.55×10^5 (based on actual chord). Data taken on an airfoil with local leading-edge sand roughness are included. Comparisons are made with analytical values of heat transfer coefficients obtained from the STAN5 boundary layer code.

Introduction

As gas turbine inlet temperatures and pressures rise, the heat loads to the turbine increase. Additional heat loading can be caused by higher free-stream turbulence intensity and greater surface roughness. Consequently more complex turbine vane cooling configurations are needed to provide acceptable metal temperatures and component life. The attainment of accurate metal temperature predictions and effectively cooled and durable parts requires accurate knowledge of high-resolution heat transfer coefficients. A common method used to determine these coefficients consists of finite heater strips with thermocouples (refs. 1 and 2). This method, however, only provides average heat transfer coefficients over intermittent selected areas and is generally used in one-dimensional idealizations of the problem.

In this study a liquid-crystal, heater-element composite sheet was used on a large-scale turbine vane airfoil as a method for measuring high-resolution heat transfer coefficients at near-room-temperature conditions. The investigation was conducted at relatively low cost, and the inlet Reynolds number of typical high-temperature turbines was preserved. The effects on heat transfer of high free-stream turbulence intensity and vane leading-edge surface roughness, more typical of a real engine environment, were also measured. Reference 3 reports on the potential of using this method for obtaining heat transfer measurements, and reference 4 presents quantitative, continuous heat transfer coefficients obtained by this method for a model turbine blade.

Liquid crystals, by virtue of their property of changing color with temperature, provide a means of measuring continuous temperature and visualizing thermal patterns (ref. 5). By applying liquid crystals to a uniform heater and using a heat balance along with the measured electrical input power the local heat transfer coefficient and its distribution can be measured.

The unique features of the composite sheet used for this study are its simplicity and uniformity and the use of commercially available materials. This composite sheet was wrapped around the airfoil of the test vane. The tests were run at room temperature and pressure. The gas-stream inlet Reynolds number varied from 1.20×10^5 to 5.55×10^5 (based on actual chord).

This report presents quantitative, experimental heat transfer coefficients measured around a three-times-size model of a typical high-temperature gas turbine vane airfoil by using a liquid-crystal, heater-element composite sheet. Measurements of high free-stream turbulence intensity and vane leading-edge roughness are included. The results are compared with results predicted by using a computer code. Since in this study the vane surface was heated and the free stream was at room temperature, the direction of heat transfer was the opposite of what it would be in a real engine with its hot free stream. Areas of high heat transfer in this study resulted in lower surface temperatures.

Symbols

A heated area, m^2 (ft^2)

E voltage across heater sheet, V

h heat transfer coefficient, W/m^2 °C (Btu/hr ft^2 °F)

I current through heater sheet, A

Figure 1.—Schematic of test facility.

L vane surface distance from leading-edge stagnation point to trailing edge, cm (in.)

Q heat flux, W (Btu/hr)

T temperature, °C (°F)

X vane surface distance from leading-edge stagnation point, cm (in.)

Subscripts:

a air

c liquid crystal at calibrated color temperature

e electric power input

ℓ losses

Apparatus

Room-temperature air was drawn through the test facility tunnel (fig. 1), which except for the inlet and flow straightener sections was made of clear acrylic plastic and was 15.2 cm (6.0 in.) high and 68.58 cm (27.0 in.) wide. Tailboards ensured periodicity at the vane row exit. The tunnel could handle 7.8 kg/sec (17.3 lb/sec) of air with the test section installed. The maximum velocity in these tests was about 57 m/sec (187 ft/sec). This velocity produced an inlet Reynolds number of 5.55×10^5, typical of high-temperature turbines. Typical Mach numbers could not be simulated because of the velocity limitation.

A two-dimensional cascade consisting of six wooden vanes (fig. 2) was installed in the test section to simulate a turbine vane row. The vane profile was three times the size of an actual high-temperature turbine vane. The liquid-crystal, heater-element composite sheet was wrapped completely around one of the center vanes except where the copper foil bus bars were attached at the trailing-edge surface. The free-stream velocity upstream of the vanes was measured with static and total head probes.

In normal operation a soda-straw flow straightener was located 104 cm (41 in.) upstream of the vane cascade inlet to smooth the flow and to reduce turbulence. When a high turbulence level was desired, a turbulence grid was inserted 38.1 cm (15 in.) upstream of the vane cascade inlet (fig. 3). This grid consisted of 12.7-mm (0.5-in.) square bars spaced 5.33 cm (2.1 in.) apart on centers in both the horizontal and vertical directions (42-percent flow area blockage). The flow
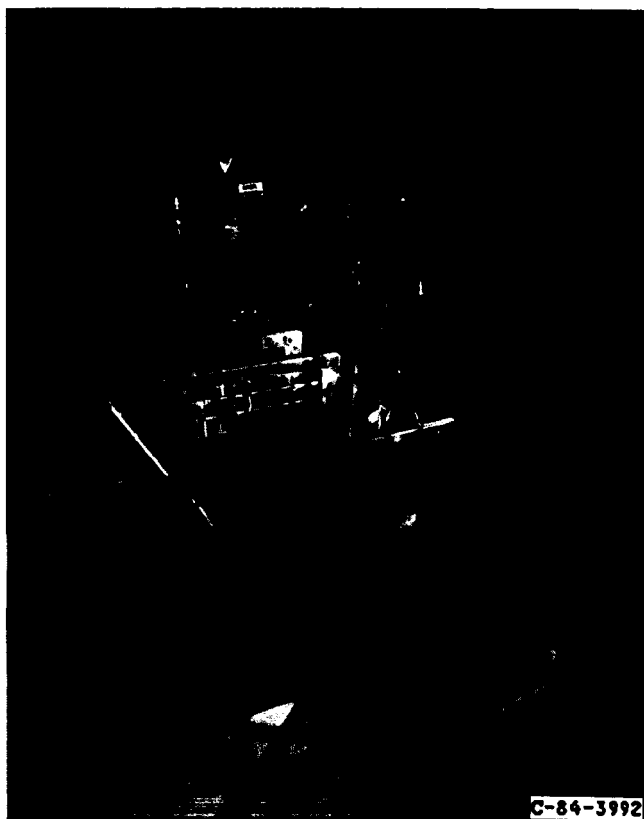

Figure 2.—Test section.
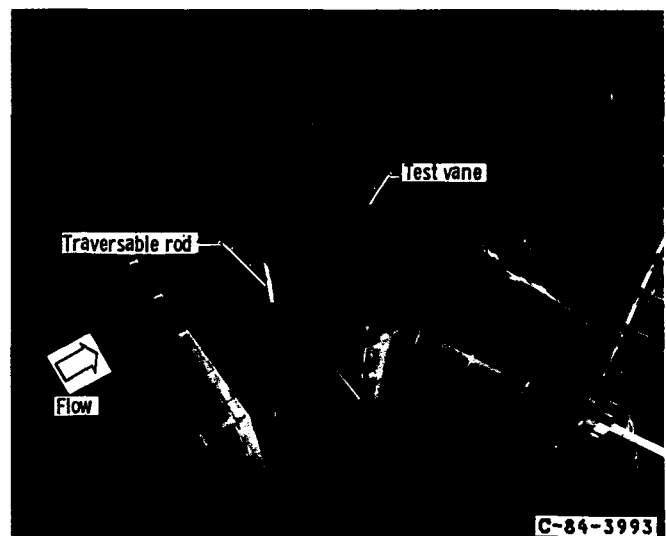
Figure 3.—Test facility with turbulence grid installed upstream of test section.

straightener and the grid were not used concurrently. To produce an upstream flow disturbance (e.g., simulating a blade trailing-edge effect), a vertical rod was located upstream. In one of the tests a stationary vertical rod 12.7 mm (0.5 in.) in diameter was placed in the flow stream 97.8 cm (38.5 in.) upstream of the vane row. This rod was used with and without a flow straightener. In another test a traversable vertical rod 12.7 mm (0.5 in.) in diameter was placed in the flow stream 19.0 cm (7.5 in.) upstream of the vane row. This rod was used both with and without the turbulence grid.

The liquid-crystal, heater-element composite sheet was composed of several layers (fig. 4). A double-coated adhesive material bonded the liquid-crystal sheet to the heater-element sheet. The same type of adhesive bonded the composite sheet to the surface of the test vane. The total thickness of the composite was 0.53 mm (0.021 in.). The 0.20-mm (0.008-in.) thick liquid-crystal sheet was purchased commercially. It consisted of cholesteric liquid crystals, which change color with temperature, laid on transparent Mylar and covered by a black plastic sealing material. The heater element, also purchased commercially, consisted of a vapor-deposited coating of gold on a 0.13-mm (0.005-in.) thick polyester sheet with a resistivity of 3.3 Ω/square (resistance of any square-shaped area). Copper foil bus bars were attached to the heater sheet at the trailing edges of each of the vane surfaces, and a conductive silver paint was used to ensure good electrical

contact. A controllable electric power source capable of 150 V at 12 A supplied electric energy to the copper foil bus bars.

To determine the effect of surface roughness on heat transfer, sandpaper grains were used on the test vane. The sand roughness was produced by using abrasive particles removed from a 60-grit garnet paper having a water-soluble adhesive. According to the Tyler standard screen scale these particles would have a nominal diameter of 0.241 mm (0.0095 in.). The particles were rinsed to remove the water-soluble adhesive and were then attached to the vane leading edge by sprinkling them on a thin, wet coat of clear lacquer (fig. 5). A second thin coat of lacquer was then sprayed on top to anchor the particles to the surface. The particles covered the circular part of the leading-edge area, which extended from 51° on the suction side to 32° on the pressure side, relative to the stagnation point. These locations corresponded to surface distances from the stagnation point of 14.0 mm (0.55 in.) and 8.9 mm (0.35 in.), respectively.

The color locations on the vane were established by a set of grid lines drawn directly on the liquid-crystal surface with
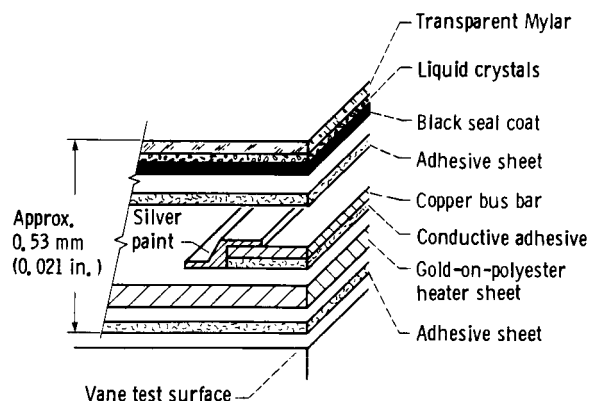

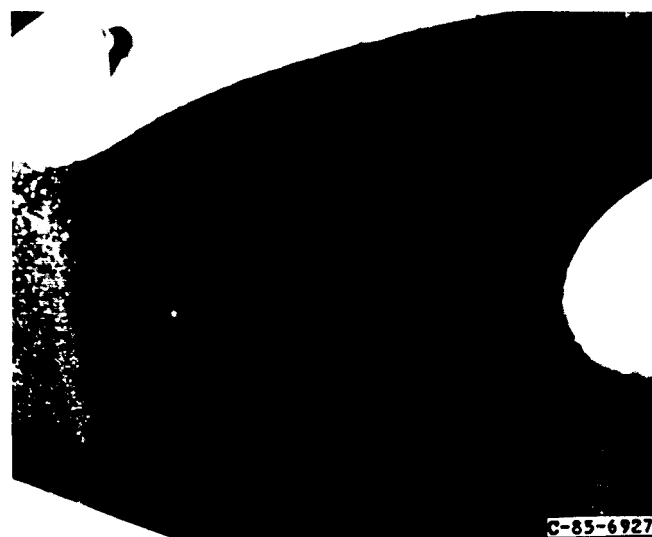Figure 4.—Cross section of liquid-crystal, heater-element composite sheet.

Figure 5.—Surface temperature patterns with leading-edge sand roughness. Reynolds number, 3.70 × 10^5.

a black permanent marker pen. The distance between lines was 12.7 mm (0.5 in.), except nearer the leading edge, where it was 5.08 mm (0.2 in.). These lines, although barely visible on the unheated surface, showed up vividly on the heated, colored surface (fig. 5).

Procedure

Experimental Heat Transfer Coefficients

The heat transfer coefficient on a vane surface was derived from an energy balance on the vane airfoil model:

$$Q_e - Q_\ell = hA(T_c - T_a) \tag{1}$$

From the measured heat input Q_e to the sheet (less the heat losses Q_ℓ), the heated area A, and the free-steam air temperature T_a the local heat transfer coefficient h was calculated at the location of the calibrated color (yellow) band (an isotherm having a uniform heat transfer coefficient produced by a uniform heat flux). The total heat energy Q_e supplied to the heater sheet was calculated from the measured voltage E across the heater sheet and the current I through a shunt resistor in series with the heater sheet. The heater current was calculated from the measured voltage across a shunt resistor having a known resistance. The heat energy loss Q_ℓ is due to conduction through the vane and radiation from the vane. The area A is the measured heated area of the heater sheet. The temperature of the calibrated color (yellow) band T_c in the liquid-crystal sheet was determined from a water-bath calibration. A temperature drop existed through the Mylar layer between the liquid-crystal-indicating temperature T_c and the actual Mylar surface temperature. This temperature drop was calculated from the known heat flux, thermal conductivity, and thickness for the Mylar layer and was subtracted from T_c in equation (1). The temperature of the upstream, inlet free-stream air T_a was measured by the same precision resistance digital thermometer used to calibrate the liquid-crystal color band.

Calibration

The liquid-crystal sheet was calibrated for correspondence between the color (yellow) and the temperature and for uniformity by immersing the sheet in a hot water bath and observing and photographing the color changes as the water gradually cooled to room temperature. The water bath was stirred before taking each temperature measurement and photograph. The water temperature was measured by a precision resistance digital thermometer. Blue corresponded to the highest temperature; green, yellow, reddish-brown, and black to decreasing levels of temperature. As discussed in references 3 and 4 yellow occurred over the narrowest temperature band. Therefore yellow was used as the calibration temperature.

The accuracy of the heat transfer coefficient depends on the uniformity of the heater-element sheet. To measure the uniformity of the heat flux produced by the heater sheet, a preliminary composite sheet was made. This sheet consisted of a liquid-crystal sheet with a very uniform yellow-temperature response (from the water-bath calibration) and a heater-element sheet. The sheet was larger than the test vane. Electric power was supplied through copper bus bars to the sheet while it was suspended horizontally in a dead air space. Voltage measurements (ref. 3) were used to calculate the percentage by which the local heat flux deviated from the average heat flux of the sheet. The area with the most uniform yellow distribution by visual observation (and hence uniform temperature and heat flux) in the sheet was then used on the test vane. The uniformity of the portion selected for use is given in the section "Results and Discussion."

Experience with liquid crystals has indicated that viewing angle and incident light angle have some effect on the resultant color (refs. 3 and 4). Photographs taken during those studies showed what effects these angles have on the liquid-crystal sheet heated to produce yellow. For angles between the camera-view and the strobe-aiming directions of less than 30° the yellow does not change significantly regardless of the angle of the liquid-crystal sheet. For angles greater than 30° the color shifts from yellow toward blue, erroneously indicating a temperature greater than that of the calibrated yellow. For this reason the tests for this study were conducted at included angles less than 30°.

Experience in this study has also shown that the calibrated yellow temperature may drift with time. For example, when a liquid-crystal sheet was bonded to a Temsheet heater (a porous material) with the double-sided adhesive material, the yellow temperature drifted downward with time (i.e., 2.1 deg C (3.7 deg F) in 27 months). However, when a liquid-crystal sheet was bonded to the vapor-deposited gold-on-polyester sheet (an airtight material) used in this study, no temperature-calibration shift was measured after 7 months. Therefore it is important to know whether the liquid crystals (on the back of the transparent Mylar sheet) are sealed and protected from the long-term damaging effects of exposure to air. It is also important to protect the liquid crystals from the damaging effect of ultraviolet light. Acrylic plastic prevents ultraviolet light transmission.

Testing

Tests were performed in several modes: (1) with a soda-straw flow straightener at the inlet and no turbulence grid, (2) with a turbulence grid but no flow straightener, (3) with neither a flow straightener nor a turbulence grid, (4) with vane surface roughness and a turbulence grid, (5) with vane surface roughness but no turbulence grid, (6) with a traversable rod both downstream of the turbulence grid and upstream of the vanes but no flow straightener, (7) with a traversable rod upstream of the vanes and a flow straightener but no grid,

(8) with a stationary rod upstream of the vanes and a flow straightener, and (9) with a stationary rod but no flow straightener.

Before the liquid-crystal heat transfer tests were performed, free-stream turbulence intensity levels were established for some of the modes of testing: (1) with a flow straightener but no turbulence grid, (2) with a grid but no straightener, and (3) with neither a grid nor a straightener. The measurements were made with a hot-wire anemometer at three free-stream Reynold numbers (based on actual chord), 1.20×10^5, 2.05×10^5, and 3.70×10^5. The results of these tests are given later.

Heat transfer tests were made at four free-stream Reynolds numbers, 1.20×10^5, 2.05×10^5, 3.70×10^5, and 5.55×10^5. The procedure was to first bring the tunnel to the desired velocity as measured by the total and static pressure probes in order to produce the proper Reynolds number. Electric power was then supplied to the composite sheet, raising its temperature to the point at which the colors began to appear. The power input was "fine tuned" to obtain the desired calibrated yellow in the locations of interest. The location of the yellow band was varied over the airfoil surface by changing the heat input while free-stream velocity remained the same.

Sufficient time had to be given to allow the temperatures and the yellow band to stabilize. Typically the first data point in a series of test runs was not taken until about 1 hr had elapsed at one combination of Reynolds number and electric power input. Thereafter data points were taken every 20 to 30 min. Data were in the form of color transparencies (which give consistent color balance results) taken with a 35-mm camera to record the yellow locations and the simultaneous documentation of air velocity, power input, air temperature, and pressure. The location of the yellow band was established by the grid-coordinate lines drawn on the composite sheet covering the vane surface.

Analytical Heat Transfer Coefficients

It is useful to compare the results of any experimental technique with analytical results. The primary tools for an analytical simulation were the STAN5 boundary layer code (refs. 6 and 7) and the measured inlet flow conditions. The velocity profiles were derived from the measured pressures. Several models and assumptions were available as to the location and type of transition from laminar to turbulent boundary layer flow. We chose an existing transition model rather than force transition in order to bracket the range of possible heat transfer coefficients (ref. 8).

In this experiment as in most low-temperature tests the hot test model was cooled by an air stream. The concern exists as to whether these results are applicable to real engines, where the component is subjected to a hot gas stream. Since the nature of this experiment prevented a reverse heat flux test, a reverse heat flux effect was examined by the analytical simulation.

The liquid-crystal, heater-element composite sheet produces a constant heat flux for a single test point but different heat flux levels for an entire heat transfer coefficient map. The effect that these differences in heat flux levels might have on the heat transfer coefficient was examined by comparing the analytical simulations based on the minimum and maximum heat fluxes needed to map the complete vane surface.

Results and Discussion

Pressure Distribution

The pressure distribution around the midspan of the airfoil surface was measured at two free-stream velocities, 19.8 and 36.6 m/sec (65 and 120 ft/sec). Pressures were measured at 24 locations by using a Scannivalve system. A plot of the results at a free-stream velocity of 36.6 m/sec (120 ft/sec) (fig. 6) shows a possible small adverse pressure gradient on the pressure surface near the leading edge.

Turbulence

Free-stream turbulence intensity was surveyed at the inlet to the vane cascade for both tunnel conditions, low turbulence with a flow straightener and fine screens and high turbulence with a coarse grid.

For the first condition the variation in free-stream turbulence intensity was measured 85.1 cm (33.5 in.) downstream of the flow straightener (fig. 7). The envelope, containing six consecutive vertical surveys, shows a consistent and repeatable pattern in the turbulence variation caused by the flow straightener. A time-averaged value at the midchannel position was 0.6 percent. When turbulence intensity was surveyed with the flow straightener removed, no pattern was observed although the average value was greater (1.4 percent). We
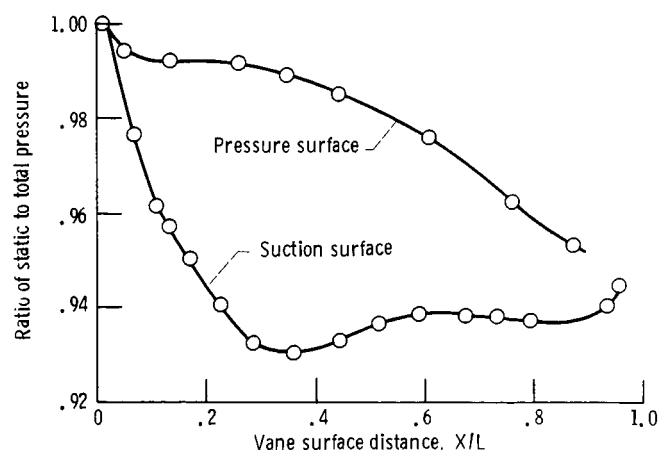

Figure 6.—Measured pressure distribution around vane. Free-stream velocity, 36.6 m/sec (120 ft/sec); Reynolds number, 3.70×10^5; temperature, 23.6 °C (74.5 °F); pressure, 96.69 kPa (14.023 psia).
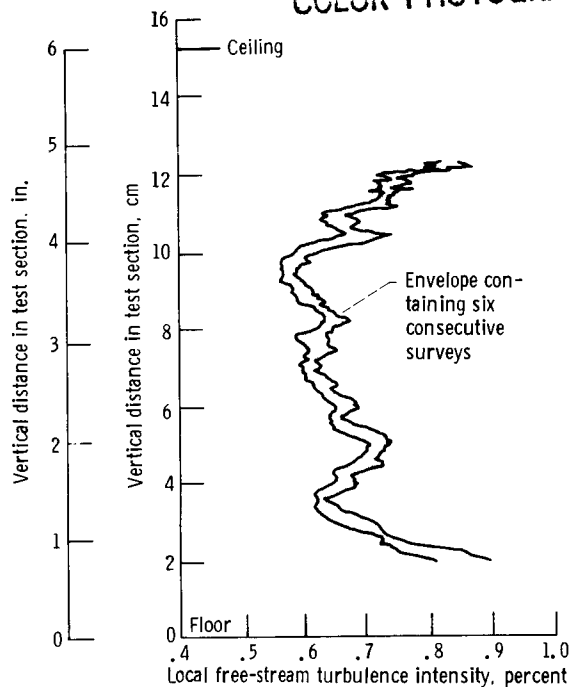
Figure 7.—Vertical survey of free-stream turbulence intensity 85.1 cm (33.5 in.) downstream of flow straightener. Velocity, 36.6 m/sec (120 ft/sec).

believe that these streak patterns are produced by neither Taylor-Goertler vortices (pressure surface) nor Tollmien-Schlichting waves (suction surface).

Surveys of pressure differences used for calculating velocities were also made. Pressure profiles (velocity) taken 6.1 cm (2.4 in.) downstream of the flow straightener did show similarly shaped patterns as those for turbulence, but pressure profiles (velocity) taken 85.1 cm (33.5 in.) downstream of the flow straightener were flat.

No significant pattern in the turbulence intensity was observed 19.0 cm (7.5 in.) downstream of the coarse turbulence grid. The average free-stream turbulence intensity measured was 17.5 percent. According to references 9 and 10 this turbulence intensity would decay to 10.0 percent at the vane cascade inlet, another 19.0 cm (7.5 in.) downstream. The distance between the grid and the vane leading edges was 30 square-grid-bar sizes. At this distance downstream and so close to the turbulence grid there may have been some nonuniformity in the velocity profile (ref. 10). However, variation in the temperature patterns, as was observed for low turbulence when using the flow straightener, was not observed in the photographs of the liquid-crystal, heater-element composite sheet for this high-turbulence environment behind the grid.

Experimental Heat Transfer

To map the entire vane airfoil surface, three views were required: the pressure side, the leading edge with the upstream portion of the suction side, and the downstream portion of the
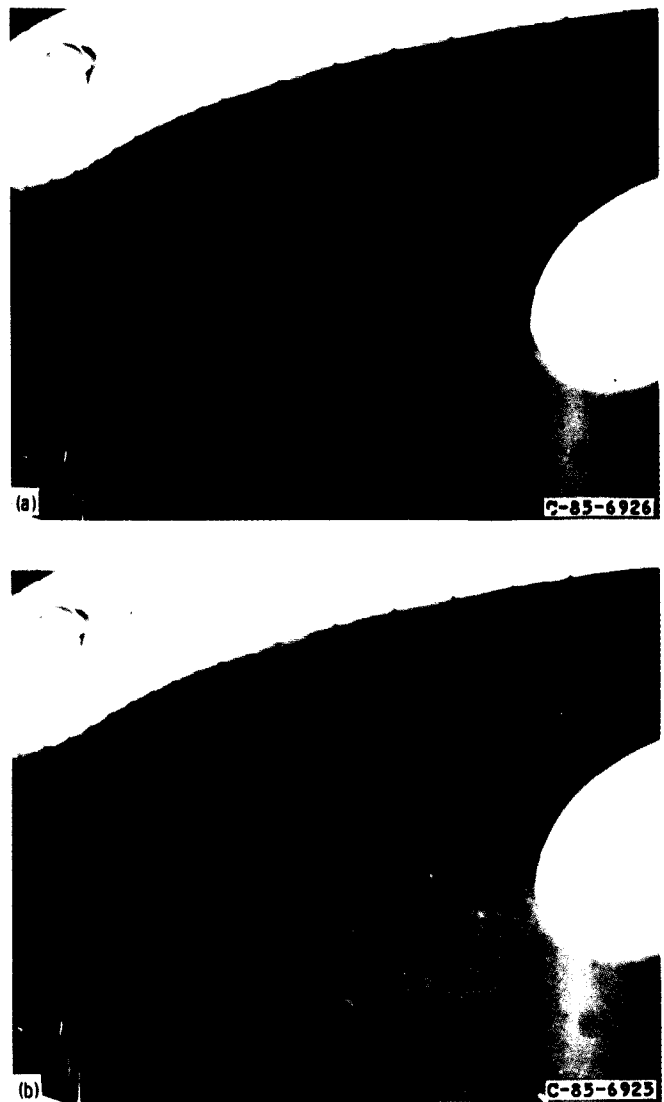
(a) Without rod in free stream.
(b) With rod in free stream 19.0 cm (7.5 in.) upstream of vane.

Figure 8.—Temperature patterns. Free-stream turbulence intensity, 0.6 percent; Reynolds number, 2.05×10^5.

suction side. The electric power was varied in the three views as needed to show the yellow bands (constant heat transfer coefficients) over the entire surface at each Reynolds number. A narrow yellow band indicates a large gradient in temperature (heat transfer coefficient).

Rod-in-free-stream turbulence effects.—With no rod in the free stream (fig. 8(a)) a large high-temperature pattern on the vane pressure surface produced a yellow-band heat transfer coefficient of 101 W/m^2 °C (17.8 Btu/hr ft^2 °F). A 12.7-mm (0.5-in.) diameter rod (which might simulate a blade trailing-edge effect) was then positioned in the stream 19.0 cm (7.5 in.) upstream of and spanwise to the vane pressure surface. The greater turbulence caused by the rod resulted in a smaller hot area (fig. 8(b)). The heat transfer over the pressure surface rose significantly. When the experiment was

repeated with the rod located 97.8 cm (38.5 in.) upstream of the vane, the smaller hot area remained. When the turbulence grid was installed to produce 10-percent turbulence intensity at the vane location (leaving the rod upstream), the smaller hot area also remained for the same heat flux and Reynolds number values as before. With the rod moved to 19.0 cm (7.5 in.) upstream of the vane pressure surface there was no further increase in the heat transfer from the pressure surface. It appeared that the turbulence generated by the grid was not significantly increased by the turbulence generated by the rod. In general when the free-stream turbulence intensity was increased, the heat transfer rose (ref. 11). Therefore it is important in heat transfer studies, which simulate real-engine conditions, to consider the real turbulence intensity level.

Particle-on-surface disturbance effects.—The spanwise cyclic pattern near the trailing edge in a small-temperature-

(a) Without particle on surface.
(b) With particle on surface.

Figure 9.—Cyclic pattern resulting from upstream flow straightener. Free-stream turbulence, 0.6 percent; Reynolds number, 5.55 × 10⁵.

gradient region (fig. 9) is an example of the variation in heat transfer caused by flow-straightener-induced turbulence. This cyclic pattern (shown in ref. 4) was not observed here in the high-turbulence-intensity environment at a downstream distance as small as 30 square-grid-bar sizes. Note that in the high-temperature-gradient region toward the leading edge the turbulence-induced cyclic pattern is not significant. At this test condition a sharp temperature pattern appeared (fig. 9(b)) near the top of the vane at a chordwise position of 5.1 cm (2.0 in.). Examination revealed the presence of a very small particle stuck on the vane surface. The particle caused a narrow wake in the downstream temperature pattern and a high gradient in the heat transfer. This demonstrates how a seemingly insignificant disturbance can adversely affect experimental results. Morkovin discusses such "bypass" mechanisms to turbulence in reference 12. When the particle was removed, the original temperature pattern returned. The pattern produced by the wake might have gone unnoticed if thermocouples had been used instead of liquid crystals with their high-resolution capability.

Experimental Corrections

Before quantitative experimental heat transfer coefficients could be obtained, five calibrations and corrections had to be made to the data. The techniques used are considered part of the results in this report. First, the heat flux was not uniform because the resistance of the heater sheet was not uniform. Second, changes in temperature changed the resistivity of the heater sheet because of its thermal coefficient of resistivity. Third, repeated thermal cycles during testing, which caused the vapor-deposited gold on the polyester to yield (or stretch) irreversibly, raised heater resistance. Fourth, the flow-straightener-induced turbulence produced a spanwise variation in the temperature (and heat transfer coefficient). And fifth, some nonconvection losses were included in calculating the heat transfer coefficient.

Nonuniform heater resistance.—The nonuniform heating of the heater sheet was minimized to an accepted ±6.0 percent by selecting the most uniform vapor-deposited gold material according to the procedure discussed in references 3 and 4.

Temperature-dependent heater resistivity.—The thermal coefficient of resistivity was determined from resistance measurements taken on the heater sheet over a range of temperatures. The resistivity was found to increase 0.134 percent/deg C (0.074 percent/deg F). From the current and voltage readings needed to map the airfoil at a given Reynolds number the average resistances of the heater sheet varied by ±1.25 percent. This corresponded to a variation of 10 deg C (18 deg F) in average heater-sheet temperatures. Conversely any local variation in heater-sheet temperature varied the local resistance, which in turn varied the local heat flux. The local heat flux at the yellow constant-temperature band was not necessarily the average heat flux of the whole heater sheet because the yellow constant temperature (and local
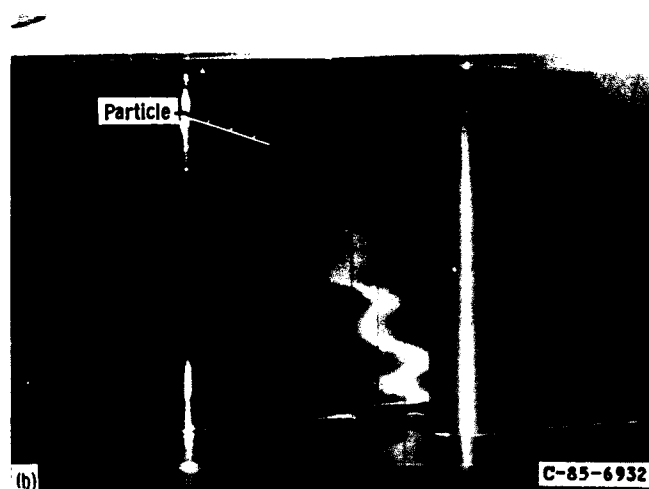
7

resistance) was not necessarily the average temperature (and average resistance) of the whole heater sheet. Thus an error band of 1.25 percent would have existed in the heat transfer coefficient because of the variation in the heat flux produced by the variation in the temperature-dependent resistance. To correct for this temperature-dependent resistance variation, the actual resistance at the calibrated yellow temperature of 40.9 °C (105.6 °F) had to be used.

Time-variant heater resistance.—The heater-sheet resistance was found to increase by 8.2 percent over the testing time period. This was apparently caused by the repeated temperature cycles stretching the vapor-deposited gold layer thinner with time. Fortunately a plot of average heater-sheet resistance measured for each test point showed only three resistance values during the testing time period. By using the measured room-temperature resistance along with the
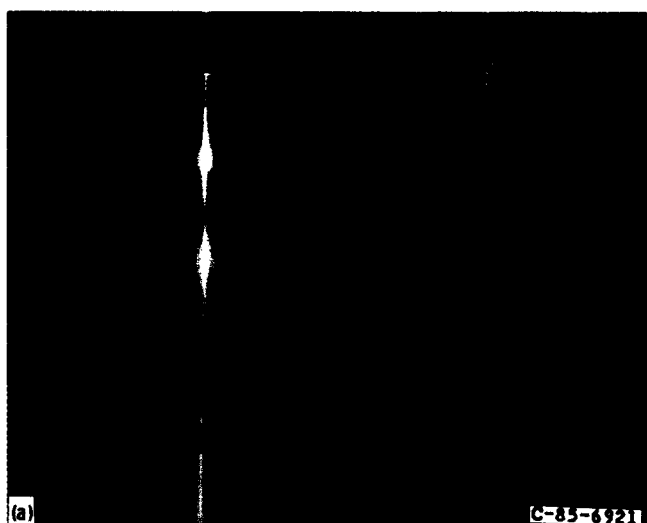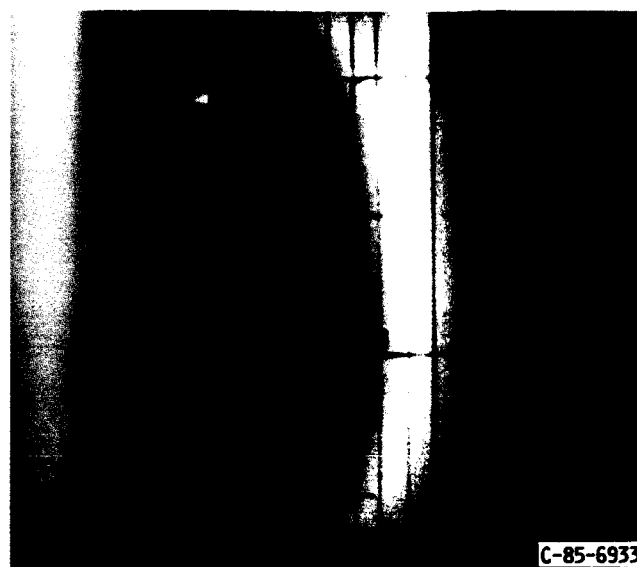

Figure 11.—Leading-edge temperature pattern for nonconvection heat loss measurement. No airflow.

calibrated thermal coefficient of resistivity, and assuming that the stretching was uniform over the airfoil, the local resistance of the yellow band (and therefore the corresponding heat transfer coefficient) was corrected for each data point.

Spanwise-varying heat transfer coefficient.—The spanwise variation in the heat transfer coefficient, caused by the flow-straightener-induced turbulence and observed in the low-temperature-gradient regions of the vane, was measured in the same way as the heater-sheet nonuniformity. That is, two heat flux measurements were used for the low-temperature-gradient region on the pressure surface at a given flow condition (fig. 10): the lowest value that showed the first streaks of the calibrated yellow temperature, and the highest value that showed the last remaining streaks of the calibrated yellow temperature. The corresponding calculated minimum and maximum heat transfer coefficients varied by ±5.0 percent about the average of these two values. In this study, however, only spanwise-averaged heat transfer coefficients are presented.

Nonconvection heat losses.—To eliminate spanwise heat conduction loss, the yellow locations were selected near the vane midspan. In an effort to approximate a worst case of all other heat losses (radiation and conduction through the vane-chord plane) the total heat input for a no-airflow condition was measured. Then the calculated free-convection heat loss was subtracted from this total (ref. 4). The calculated heat loss due to heat radiation (the emissivity of the Mylar surface measured 0.89) was then found to exactly equal the remaining amount. That is, the maximum heat loss (at the vane leading edge) for the no-airflow condition (fig. 11) exactly equalled the sum of the heat losses due to free convection and radiation. Therefore any conduction heat loss through the vane-chord plane was considered negligible and was neglected. The temperature drop was calculated and corrected through the Mylar layer (between

(a) Low heat flux.
(b) High heat flux.

Figure 10.—Spanwise-varying heat transfer coefficient. Flow straightener 104 cm (41 in.) upstream; Reynolds number, 2.05 × 10⁵.

the liquid-crystal-indicating temperature T_c and the actual Mylar surface temperature). The error in the calculated heat transfer coefficient due to the experimental measurements in the test facility (current, voltage, pressure, temperature, and dimensions) was ±0.2 percent. This maximum error was caused by the variation in the heater-sheet heat flux (±6 percent) due to its nonuniform resistance. Combining all uncorrected errors gave a maximum error in the experimental heat transfer coefficient of ±6.2 percent.

Once these calibration and correction techniques were explored, the composite was ready to be used for obtaining quantitative heat transfer coefficients.

Experimental Heat Transfer Coefficients

The major objective of this program was to map the quantitative heat transfer coefficients with vane surface distance. Heat transfer coefficients h (ignoring the small, uncorrected conduction heat loss through the vane-chord plane) were calculated as a function of dimensionless vane surface distance X/L for four inlet free-stream Reynolds numbers (1.20×10^5, 2.05×10^5, 3.70×10^5, and 5.55×10^5, based on actual chord), for a low (0.6 percent) and a high (10 percent) free-stream turbulence intensity, and for a smooth and rough leading-edge surface. The rough surface was obtained by covering part of the vane leading edge with sand having a nominal diameter of 0.241 mm (0.0095 in.). The effects of Reynolds number, turbulence intensity, and leading-edge roughness are discussed separately.

Reynolds number effects.—The influence of Reynolds number on h was determined for both low and high turbulence intensities (fig. 12). (The experimental data points are connected by lines only to improve readability.) Generally for a given turbulence intensity h increased with Reynolds number. At the leading edge h was very high, but it dropped to a minimum on the pressure surface, where the boundary layer was laminar (except for the higher Reynolds numbers, where the start of transition occurred). On the suction surface h reached a peak near the leading edge, decreased with surface distance to a minimum at the start of transition, and then increased rapidly near the trailing edge, where the flow was no longer guided by the neighboring vane. For the high-turbulence free stream at the suction-surface trailing edge (having a turbulent boundary layer), h was proportioned to the Reynolds number to the 0.8 power, as expected.

Free-stream turbulence effects.—At a Reynolds number of 1.20×10^5 (fig. 13(a)) the h at the leading edge was 31 percent greater for the high- than for the low-turbulence free stream. The pressure-surface boundary layer remained laminar. The leading-edge roughness effects are discussed separately (denoted by solid symbols in the figures). On the suction surface the distance from the leading-edge stagnation point to the transition starting point for the high-turbulence free stream was 78 percent of the low-turbulence distance. The minimum h was 72 percent greater for the high-turbulence free

stream. For that free stream only, the beginning of the turbulent boundary layer at the suction-surface trailing edge ($X/L > 0.69$) had a flat-h profile. A similar flat-h profile was observed for a blade airfoil reported in reference 4.

At a Reynolds number of 2.05×10^5 (fig. 13(b)) the h on the leading edge was greater for the high-turbulence free stream by 28 percent. The pressure-surface boundary layer also remained laminar. On the suction surface the transition starting-point distance for the high-turbulence free stream was
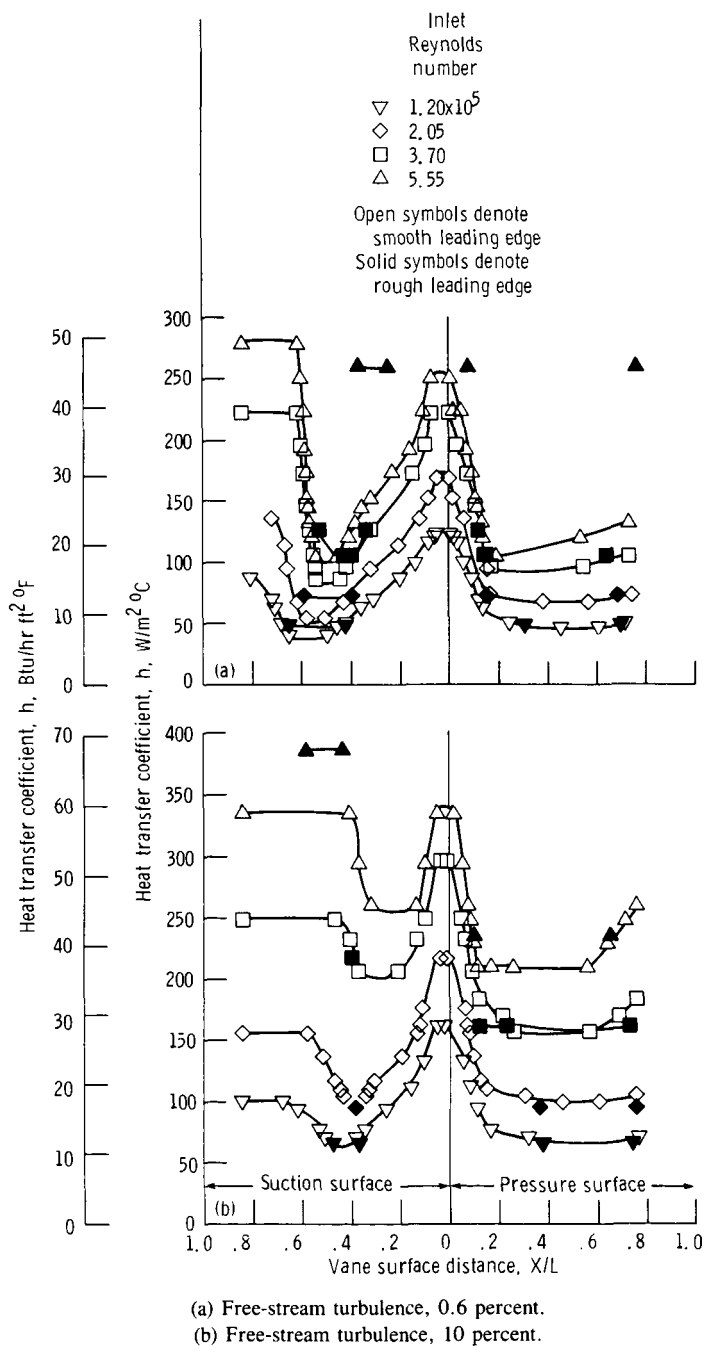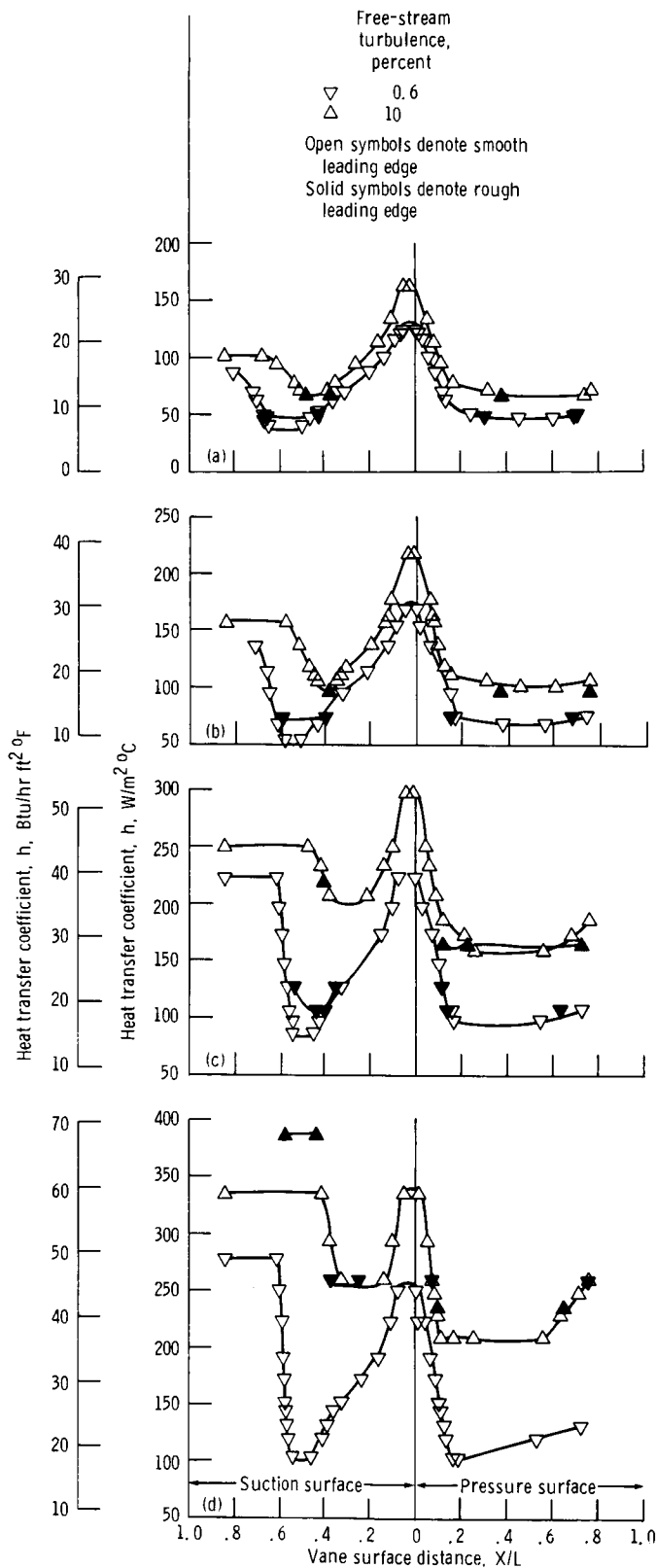

(a) Free-stream turbulence, 0.6 percent.
(b) Free-stream turbulence, 10 percent.

Figure 12.—Heat transfer coefficient map for low and high free-stream turbulence.

(a) Reynolds number, 1.20 × 10^5. (c) Reynolds number, 3.70 × 10^5.

(b) Reynolds number, 2.05 × 10^5. (d) Reynolds number, 5.55 × 10^5.

Figure 13.—Heat transfer coefficient map for various Reynolds numbers.

72 percent of the low-turbulence distance. The minimum h was 92 percent greater for the high-turbulence free stream. For that free stream only, the beginning of the turbulent boundary layer near the suction-surface trailing edge also had a flat-h profile ($X/L > 0.58$).

At a Reynolds number of 3.70×10^5 (fig. 13(c)) the leading-edge h was greater for the high-turbulence free stream by 33 percent. Transition began in the pressure-surface boundary layer. On the suction surface the transition starting-point distance for the high-turbulence free stream was 59 percent of the low-turbulence distance. The minimum h was 139 percent greater for the high-turbulence free stream. The flat-h profile was present for both turbulence levels. The high-turbulence flat-h profile was 12 percent greater than, and started at 76 percent of the surface distance for, the low-turbulence flat-h profile. This indicates that the transition to a turbulent boundary layer started sooner for the high-turbulence free stream.

At the maximum Reynolds number of 5.55×10^5 (fig. 13 (d)), matching a typical, real turbine vane operating condition, the leading-edge h was 34 percent greater for the high-turbulence free stream. The four data points on the pressure side for the high-turbulence free stream, having h of 209.0 W/m^2 °C (36.8 Btu/hr ft^2 °F), were obtained from the photograph shown in figure 14. These four yellow-band locations resemble the temperature (or h) pattern observed on a blade airfoil in the study of reference 4; that airfoil had a strong separation bubble near the pressure-surface leading edge. Similarly figure 14 shows a second hot region (blue) upstream between the first and second yellow bands ($0.11 < X/L < 0.17$). These double hot regions (minimum h values) apparently show that downstream of an adverse pressure gradient a favorable pressure gradient (accelerating free stream) suppressed the tendency toward transition and kept the boundary layer laminar. This four-yellow-band pattern was only observed on the smooth-surface vane operating at the maximum Reynolds number. Transition began in the pressure-

Figure 14.—Temperature pattern showing weak separation near leading edge. Reynolds number, 5.55 × 10^5.
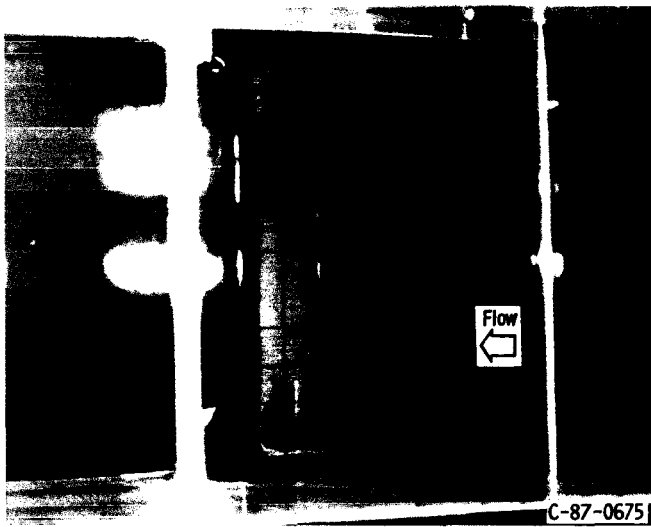
Figure 15.—Pattern showing constant temperature near trailing edge. Reynolds number, 5.55×10^5.

surface boundary layer. On the suction surface the transition starting-point distance for the high-turbulence free stream was 46 percent of the low-turbulence distance. The minimum h was 150 percent greater for the high-turbulence free stream. Therefore over the range of Reynolds numbers tested and for the high-turbulence free stream (relative to the low-turbulence free stream) the transition starting-point distance (from stagnation) decreased and the corresponding minimum h increased with increasing Reynolds number. The high-turbulence flat-h profile (at the start of the turbulent boundary layer near the trailing edge) was 20 percent greater than, and started at 66 percent of the surface distance for, the low-turbulence flat-h profile.

A wide, yellow temperature pattern (constant h) started at an X/L of 0.41 and extended to the downstream edge of the heated test sheet ($X/L = 0.84$) (fig. 15). The spanwise temperature variation in this chordwise range was due to an asymmetrical spanwise heat conduction loss. The spanwise variation in the corresponding h was not very great because of the near-constant chordwise location of the upstream edge of the spanwise yellow band. To eliminate spanwise heat conduction loss, the chordwise location of the yellow band was always taken at the knee of the band (which has no spanwise temperature gradient). The knee occurred below the vane midspan, where no spanwise heat conduction existed.

Leading-edge roughness effects.—The leading-edge sand roughness, shown in figure 5, had no noticeable effect on h at either turbulence level for the lowest Reynolds number tested (figs. 12 and 13(a)). Because the sand roughness was located only on the vane leading edge, where the boundary layer was laminar, the important parameter that would have influenced h was the critical roughness (ref. 11). The critical roughness is the height of a protuberance that will cause transition in a laminar boundary layer and move the point of transition upstream. It is a function of the kinematic viscosity and the

friction velocity (the measure of the intensity of turbulent eddying). The critical roughness calculated for the lowest Reynolds number (1.20×10^5) at the downstream edge of the sand-covered area on the suction surface was 0.363 mm (0.0143 in.). Because this value was greater than the 60-grit particle diameter of 0.241 mm (0.0095 in.), no effect would be expected. The calculated critical roughness for the pressure surface was about 11 percent less than that for the suction surface at all Reynolds numbers tested. The calculated critical roughness for the actual-size high-temperature turbine vane was 0.038 mm (0.0015 in.) at a Reynolds number of 5.55×10^5. This critical roughness was one-third of that for the three-times-size model airfoil used in this study.

The same conclusion was drawn from the roughness data at a Reynolds number of 2.05×10^5 (fig. 13(b)) because the calculated critical roughness of 0.244 mm (0.0096 in.) still did not fall below the sand roughness.

At a Reynolds number of 3.70×10^5 (fig. 13(c)) the roughness had no effect on the pressure surface in the low-turbulence free stream. In the high-turbulence free stream the presence of roughness did show a slight tendency to cause the boundary layer to transition near the leading edge, similar to the highest Reynolds number case for the smooth-leading-edge vane surface (fig. 13(d)). Because the sand roughness exceeded the calculated critical roughness of 0.155 mm (0.0061 in.), an effect of roughness on h could have been observed. The temperature (or h) pattern (fig. 5) suggests the tendency toward transition for the high-turbulence free stream at the isolated blue (hot) area bounded by the calibrated yellow bands ($0.12 < X/L < 0.23$). This tendency toward transition was not observed on the smooth leading edge for the same Reynolds number. On the suction surface the roughness did affect the low-turbulence free-stream transition starting-point distance: it was 84 percent that for the smooth-leading-edge vane surface. Roughness also increased the corresponding minimum h by 22 percent. There were no data to indicate that the leading-edge roughness had any effect on the high-turbulence, suction-surface h for Reynolds numbers to 3.70×10^5.

At the maximum Reynolds number of 5.55×10^5 (fig. 13(d)) no effect of leading-edge roughness on h was observed on the pressure surface for the high-turbulence free stream. The slight tendency for the boundary layer to transition shown by the h data at the next lower Reynolds number (3.70×10^5) was not observed here because the heat flux was set a little too high. That is, the yellow-band h was too great, and therefore the double hot regions (minimum h values) were not produced. For the low-turbulence free stream, however, the h on the pressure surface was significantly higher at the trailing edge, indicating an earlier transition toward a turbulent boundary layer. For the low-turbulence free stream on the suction surface the leading-edge roughness significantly reduced the transition starting-point distance to 62 percent of the smooth-surface distance. The critical roughness was calculated to be only 0.114 mm (0.0045 in.). The corresponding minimum h was dramatically increased by

11

150 percent. For the high-turbulence free stream the leading-edge roughness also increased the flat-h profile near the trailing edge by 15 percent of the smooth surface profile.

Generally the leading-edge roughness only had a noticeable effect on h in the presence of the low-turbulence free stream and then only at the higher Reynolds numbers, where the sand roughness exceeded the calculated critical roughness.

Analytical Heat Transfer Coefficients

A typical analytical simulation computed by the STAN5 boundary layer code for a Reynolds number of 3.70×10^5 is shown in figure 16 for both free-stream turbulence levels (0.6 and 10 percent) and both heat transfer directions (out of and into the vane surface). For all calculations except that for the high-turbulence free stream on the suction surface the transition models used were Van Driest and Blumer's (ref. 7) for the start of transition and Dhawan and Narasimha's (ref. 7) for the transition length. For the exception Seyb's model (ref. 7) was used for the start of transition. Also simulated, but not shown, was the variation in h computed by using the minimum and maximum heat fluxes needed to experimentally map the entire vane surface. The variation in the computed h resulting from varying thermal properties near the surface

Figure 16.—Heat transfer coefficient map and STAN5 analysis. Reynolds number, 3.70×10^5.

was less than the nonuniformity in the heat flux produced by the heater sheet. The maximum variation in the computed h was ±4 percent on the suction surface at the beginning of the turbulent boundary layer.

Positive Heat Transfer Simulation

The positive heat transfer simulation matched the operation of the liquid-crystal, heater-element composite sheet, in which the heat was transferred from the heated surface of the test vane to the cooler surrounding airstream. As shown in figure 16, the STAN5 boundary layer computation agreed relatively well with the experimental h for the pressure surface in a low-turbulence free stream. For the high-turbulence free stream the computed h on the pressure surface fell below the experimental h, but the values would have been greater if the pressure gradient correlation in STAN5 were replaced by a more suitable correlation. Even so, the double hot regions (minimum h values) were shown by the computation. For the low-turbulence free stream the computed h on the suction surface followed the experimental h up to the start of transition, but the boundary layer calculation remained laminar to the trailing edge. None of the STAN5 transition models would start the transition soon enough for the low-turbulence free stream. Of course, by specifying it as input data the start of transition could have been forced upstream. In agreement with reference 8 the results indicate that free-stream turbulence and pressure gradient have strong, and opposite, effects on where transition starts and on the length of the transition zone.

Negative Heat Transfer Simulation

A negative heat transfer simulation would match the turbine vane environment in a real engine, in which the heat is transferred from the hot gas stream to the cooled turbine vane. As can be seen in figure 16, the computed h for the negative heat transfer simulation generally followed the trends of the positive heat transfer simulation. For the high-turbulence free stream the computed h for the negative heat transfer simulation was up to 31 percent greater on the pressure surface (near the trailing edge) and up to 10 percent less on the suction surface (near the midchord) than that for the positive heat transfer simulation. For the low-turbulence free stream the computed h for the negative heat transfer simulation was up to 42 percent greater on the pressure surface at the midchord than that for the positive simulation (and even greater at the trailing edge because the positive simulation did not reach transition). For the low-turbulence free stream the computed h on the suction surface agreed for both simulations, but both failed to start a transition, as did the experimental data. It should be pointed out that the heat flux value used as input to the STAN5 computation was the maximum experimental value required to map the entire vane airfoil. This value exceeded the local values downstream, and therefore the maximum differences downstream in the computed h (between the two simulations) may be too great. Further study is needed to examine what
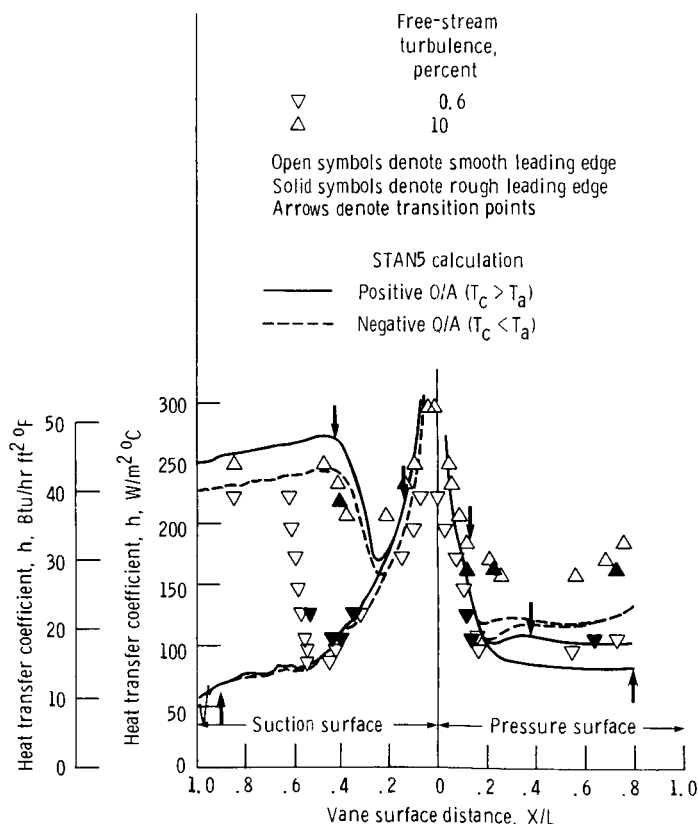
influence the direction of heat transfer (temperature gradient) has on the thermal boundary layer and the resulting h.

Concluding Remarks

The liquid-crystal technique's advantage of continuous, two-dimensional resolution was demonstrated by its ability to show the heat transfer patterns caused by the particle-on-surface disturbance, the flow-straightener-induced turbulence variation, and the effect of an adverse pressure gradient on the pressure surface near the leading edge. The maximum error in the experimental heat transfer coefficient was ±6.2 percent, and the greatest part of this was the variation in the heat flux of the heater sheet caused by its nonuniform resistance.

References

1. Florschuetz, L.W., et al., "Multiple Jet Impingement Heat Transfer Characteristics: Experimental Investigation of In-Line and Staggered Arrays with Crossflow," NASA CR-3217, 1980.
2. Van Fossen, G.J., et al., "Heat Transfer Distributions Around Nominal Ice Accretion Shapes Formed on a Cylinder in the NASA Lewis Icing Research Tunnel," AIAA Paper 84-0017, Jan. 1984.
3. Hippensteele, S.A., Russell, L.M., and Stepka, F.S. "Evaluation of a Method for Heat Transfer Measurements and Thermal Visualization Using a Composite of a Heater Element and Liquid Crystals," Journal of Heat Transfer, Vol. 105, No. 1, Feb. 1983, pp. 184-189.
4. Hippensteele, S.A., Russell, L.M., and Torres, F.J., "Local Heat-Transfer Measurements on a Large Scale-Model Turbine Blade Airfoil Using a Composite of a Heater Element and Liquid Crystals," Journal of Engineering for Gas Turbines and Power, Vol. 107, No. 4, Oct. 1985, pp. 953-960.
5. Fergason, J.L., "Liquid Crystals," Scientific American, Vol. 211, No. 2, Aug. 1964, pp. 76-85.
6. Crawford, M.E., and Kays, W.M., "STAN5: A Program for Numerical Computation of Two-Dimensional Internal and External Boundary Layer Flows," NASA CR-2742, 1976.
7. Gaugler, R.E., "Some Modifications to, and Operational Experiences with, the Two-Dimensional, Finite-Difference, Boundary Layer Code, STAN5," ASME Paper 81-GT-89, Mar. 1981.
8. Gaugler, R.E., "A Review and Analysis of Boundary Layer Transition Data for Turbine Application," ASME Paper 85-GT-83, Mar. 1985.
9. Baines, W.D., and Peterson, E.G., "An Investigation of Flow Through Screens," Transactions of the ASME, Vol. 73, No. 5, July 1951, pp. 467-480.
10. O'Brien, J.E., and Van Fossen, G.J., Jr., "The Influence of Jet-Grid Turbulence on Heat Transfer from the Stagnation Region of a Cylinder in Crossflow," ASME Paper 85-HT-58, Aug. 1985.
11. Schlichting, H., Boundary-Layer Theory, 7th ed., McGraw-Hill, New York, 1979.
12. Morkovin, Mark V., "Bypass Transition to Turbulence and Research Desiderata," Transition in Turbines, NASA CP-2386, 1984, pp. 161-180.

1. Report No.	2. Government Accession No.	3. Recipient's Catalog No.
NASA TM-87355		

4. Title and Subtitle	5. Report Date
Use of a Liquid-Crystal, Heater-Element Composite for Quantitative, High-Resolution Heat Transfer Coefficients on a Turbine Airfoil Including Turbulence and Surface Roughness Effects	
	6. Performing Organization Code
	505-62-21

7. Author(s)	8. Performing Organization Report No.
Steven A. Hippensteele, Louis M. Russell, and Felix J. Torres	E-3021
	10. Work Unit No.

9. Performing Organization Name and Address	11. Contract or Grant No.
National Aeronautics and Space Administration Lewis Research Center Cleveland, Ohio 44135	
	13. Type of Report and Period Covered

12. Sponsoring Agency Name and Address	Technical Memorandum
National Aeronautics and Space Administration Washington, D.C. 20546	14. Sponsoring Agency Code

15. Supplementary Notes

16. Abstract

Local heat transfer coefficients were measured along the midchord of a three-times-size turbine vane airfoil in a static cascade operated at room temperature over a range of Reynolds numbers. The test surface consisted of a composite of commercially available materials: a Mylar sheet with a layer of cholesteric liquid crystals, which change color with temperature, and a heater made of a polyester sheet coated with vapor-deposited gold, which produces uniform heat flux. After the initial selection and calibration of the composite sheet, accurate, quantitative, and continuous heat transfer coefficients were mapped over the airfoil surface. Tests were conducted at two free-stream turbulence intensities: 0.6 percent, which is typical of wind tunnels; and 10 percent, which is typical of real engine conditions. In addition to a smooth airfoil, the effects of local leading-edge sand roughness were also examined for a value greater than the critical roughness (the minimum roughness that causes transition in a laminar boundary layer). The local heat transfer coefficients are presented for both free-stream turbulence intensities for inlet Reynolds numbers from 1.20×10^5 to 5.55×10^5 (based on actual chord). Data taken on an airfoil with local leading-edge sand roughness are included. Comparisons are also made with analytical values of heat transfer coefficients obtained from the STAN5 boundary-layer code.

17. Key Words (Suggested by Author(s))	18. Distribution Statement
Heat transfer; Liquid crystals; Turbulence; Roughness; Heat transfer coefficients	Unclassified - unlimited STAR Category 35

19. Security Classif. (of this report)	20. Security Classif. (of this page)	21. No. of pages	22. Price*
Unclassified	Unclassified	15	A02

*For sale by the National Technical Information Service, Springfield, Virginia 22161